

Finite-Time Instabilities of Lower-Stratospheric Flow

D. L. HARTMANN,* T. N. PALMER, AND R. BUIZZA

European Centre for Medium-Range Weather Forecasts, Reading, England

(Manuscript received 4 May 1995, in final form 11 December 1995)

ABSTRACT

The linear structures that produce the most in situ energy growth in the lower stratosphere for realistic wintertime flows are investigated using T21 and T42 calculations with the ECMWF 19-level forecast model. Significant growth is found for relatively large scale structures that grow by propagating from the outer edges of the vortex into the strong jet features of the lower-stratospheric flow. The growth is greater when the polar vortex is more asymmetric and contains localized jet structures. If the linear structures are properly phased, they can induce strong nonlinear interactions with the polar vortex, both for Northern Hemisphere and Southern Hemisphere flow conditions, even when the initial amplitudes are small. Large extensions from the main polar vortex that are peeled off during wave-breaking events give rise to a separate class of rapidly growing disturbances that may hasten the mixing of these vortex extensions.

1. Introduction

Calculations of in situ instability for the zonal-mean state of the stratosphere have generally shown rather small growth rates so that local instabilities have been regarded as less important in the stratosphere compared to the troposphere. The evolution of flow in the stratosphere is thought to be strongly controlled by local radiative drive and by dynamical forcing originating in the troposphere (e.g., Hartmann 1985; Andrews et al. 1987). Nonetheless, the stratosphere appears to respond differently to forcing from below, depending on the flow configuration within it, and some modest instabilities associated with strong horizontal shears in the stratosphere have been noted (e.g., Hartmann 1983; Manney et al. 1991; Ishioka and Yoden 1994). When the stratospheric state is suitably preconditioned, forcing by planetary wave propagation from below can cause dramatic changes in the state of the stratosphere that do not occur otherwise (McIntyre 1982). The Northern Hemisphere experiences major midwinter stratospheric warmings, whereas the Southern Hemisphere never does (Schoeberl 1978). Frederiksen (1982) found that modal instabilities of the three-dimensional, zonally asymmetric state of the atmosphere prior to major warmings can have significant growth rates when the zonal-average state is stable.

In recent years some new insights have been gained by considering the growth of disturbances from an initial perturbation that is allowed to grow over a finite interval of time. In an atmosphere that evolves rapidly and in which nonlinear effects become important on timescales of a few days, it can be argued that these finite-time optimal perturbations have more practical relevance than traditional normal modes (e.g., Farrell 1982; Lacarra and Talagrand 1988; Farrell 1989; Borges and Hartmann 1992; Molteni and Palmer 1993; Farrell and Ioannou 1994; Palmer et al. 1994). In particular, given a linear tangent model that describes the evolution of perturbations about a specified time-varying flow trajectory, and given the adjoint of this linear tangent model, it is possible to calculate a subset of the most rapidly growing perturbations for quite realistic flows. Buizza et al. (1993) describe how the dominant optimal perturbations, or singular vectors, can be calculated for low-resolution versions of the ECMWF forecast model.

In this paper we examine the singular vectors for stratospheric flow by choosing the stratosphere as the region in which energy growth is to be maximized. The top three levels of a 19-level version of the ECMWF forecast model are chosen as the region where growth is optimized. These levels occur at pressures of approximately 10, 29, and 50 hPa. Because the top level of the model is near 10 hPa, it may be that the growth rates of the disturbances are exaggerated compared to what would occur for the levels chosen if the model top were at a higher level. We perform some integrations in which the top level is raised and more levels are added in the stratosphere to show that the mode structures are not overly sensitive to the exact location of the model levels, but we are unable to prove that

* Permanent affiliation: Department of Atmospheric Sciences, University of Washington, Seattle, Washington.

Corresponding author address: Dr. Dennis L. Hartmann, Department of Atmospheric Sciences, AK-40, University of Washington, Seattle, WA 98195.

these disturbances are similar to those of an unbounded atmosphere. In any case, they are the structures that grow most rapidly in a numerical weather prediction model with a typical vertical representation of the stratosphere and are relevant at least to that extent. Kalnay and Toth (1995) have also identified structures that grow efficiently in the stratosphere of the National Centers for Environmental Prediction (NCEP) model. The structures identified in the present study grow primarily through barotropic mechanisms, which is probably realistic for this part of the atmosphere, where horizontal shears are large, vertical shears are modest, and static stability is very high. It can be hoped, therefore, that these disturbances are also characteristic of an unbounded stratosphere.

For the flow conditions of the stratosphere, and with the model resolution used, the most rapidly growing disturbances are of large scale and grow primarily through propagation toward jets from regions of weak westerlies on the flanks and upstream of the jets. Despite the large scale of these disturbances, they can have strong nonlinear interactions with the vortex structure, sometimes causing very significant changes from relatively small initial perturbations. The most rapid growth occurs for those cases when the vortex is distorted to produce localized jets; therefore, rapidly growing disturbances are expected to be found during winter at those times when the vortex is strong and asymmetric.

2. Calculation of singular vectors

We provide here a very brief mathematical description of the singular vector calculation. More detailed descriptions can be found in Buizza et al. (1993) and Buizza and Palmer (1995). Denote by $A[x]$ the ECMWF nonlinear primitive equation model. The time evolution equation for a state vector x can be formally written in terms of the (M -dimensional) nonlinear evolution equation

$$\frac{\partial x}{\partial t} = A[x], \quad (1)$$

where the components of the state vector x are the spherical-harmonics expansions of vorticity ζ , divergence D , temperature T , humidity q , together with the logarithm of surface pressure π .

Consider a small perturbation x' of the state vector x , for which a linear evolution equation can be formed, which is valid for sufficiently short time intervals:

$$\frac{\partial x'}{\partial t} = A_t x', \quad (2)$$

where A_t is an approximation of the tangent linear model $\partial A / \partial x|_{x(t)}$. In fact, while a complete linearization of the model dynamics can be included, the only physical processes included in the linear operator A_t are

simplified versions of the ECMWF vertical diffusion, horizontal diffusion, and surface drag schemes (Buizza 1994). The horizontal diffusion is fourth power or biharmonic, with a coefficient chosen to give an e -folding timescale at the maximum total wavenumber of 5 days for T21 and 1.25 days for T42.

Equation (2) can be written in the integral form

$$x'(t) = L(t, t_0)x'(t_0). \quad (3)$$

The operator $L(t, t_0)$ is referred to as the forward tangent propagator; it maps small perturbations along the (nonlinear) trajectory from an initial time t_0 to some future time t . From here on we drop the ‘‘primes’’ on the perturbation quantities. If we define an inner product, which we choose to define here as an energy inner product, then we can derive the adjoint of the forward tangent propagator. This inner product defines the energy, and with the forward tangent propagator and its adjoint we may use (3) to express the linear perturbation energy at some future time t in terms of the perturbation state vector at some initial time t_0 :

$$\|x(t)\|^2 \equiv [x(t); x(t)] = [x(t_0); L^{*E}Lx(t_0)], \quad (4)$$

where L^{*E} is the adjoint of L with respect to the energy inner product. Unlike L itself, the operator $L^{*E}L$ is symmetric. Hence its eigenvectors $v_i(t_0)$ can be chosen to form a complete orthonormal basis in the M -dimensional tangent space of linear perturbations with real eigenvalues $\sigma_i^2 \geq 0$ (e.g., Noble and Daniel 1988); that is,

$$(L^{*E}L)v_i(t_0) = \sigma_i^2 v_i(t_0). \quad (5)$$

Since any $x(t)/\|x(t_0)\|$ can be written as a linear combination of the set $v_i(t)$, it follows that

$$\max_{x(t_0) \neq 0} \left[\frac{\|x(t)\|}{\|x(t_0)\|} \right] = \sigma_1. \quad (6)$$

The σ_i , ranked in terms of magnitude, are called the singular values of the operator L , and the vectors $v_i(t)$ are called the singular vectors of L . Maximum energy growth over the time interval $t - t_0$ is therefore associated with the dominant singular vector: $v_1(t_0)$ at initial time and $v_1(t)$ at optimization time. In addition, a local projection operator may be added to the model operator, which will constrain the singular values to be based on a maximization of the final state energy in a restricted geographical region (Buizza and Palmer 1995).

In this study, the singular vectors were selected to maximize the perturbation energy at the optimization time in the top three model levels at about 10, 29, and 50 hPa and in a geographical region that includes either the northern or southern polar cap beginning at the equator, or in one case at 10° latitude. A selection of the most rapidly growing, or dominant, singular vectors can be obtained through an iterative Lanczos algorithm (Buizza et al. 1993). In all of the computations de-

scribed here, the optimization time was taken to be two days. The basic experiments described here were performed with a 19-level, T21 version of the model (T21L19), although some singular vector calculations with T42L19 and T42L25 versions, and some time integrations with the nonlinear, full physics T63 version of the ECMWF forecast model will also be described.

3. Vertical and horizontal structure of singular vectors

We discuss first the vertical structure of the disturbances and then their horizontal structure. The vertical structure is largely determined by the choice of optimization volume, which is confined to the top three levels of the model, and to the optimization time, which is chosen to be two days. For an optimization time of two days, the disturbances originate locally in the stratosphere and will achieve their peak energy near the top of the model. With these calculations we are therefore seeking initial perturbations that originate in the lower stratosphere and result in rapid growth of energy there. To survey the dependence of growth rate on atmospheric structure, we have calculated the singular vectors about every two weeks during the Northern Hemisphere winter 1992/93 and the Southern Hemisphere winter 1992. The vertical structures of the initial and final energies averaged over the first six singular vectors for particular cases are shown in Fig. 1. In all cases we examined (about 20) the general structure is the same, with both the initial and final energy peaked at the top model level. In the case of the Southern Hemisphere stratosphere, the initial amplitude extends over a slightly deeper layer, probably because the strong shears extend over a deeper layer there. In the Northern Hemisphere the strongest shears resolved by the model are very near the 10-hPa level.

The total spherical harmonic wavenumber energy spectra of the singular vectors at initial and final time are shown in Fig. 2 for six representative cases from the Northern Hemisphere (NH) and Southern Hemisphere (SH) winters. Three cases of relatively rapid growth are shown: (a) 15 December 1992, (b) 1 January 1993, and (c) 14 February 1993 in the NH, along with three cases of relatively slow growth; (d) 1 February 1992 in the NH, (e) 14 June 1992, and (f) 28 June 1992 in the SH. These cases bracket the range of growth that was observed in a larger sample of dates from two winters in each hemisphere. In the cases of rapid energy growth in the NH, the initial energy peaks at the highest resolved wavenumber (21), while the final energy peaks near total wavenumber 7. In the cases of weak growth the initial energy peaks around wavenumber 8 or 10, and the final energy peaks around total wavenumber 5. The final energy spectra are significantly different from those typically observed in the troposphere, where the final energy usually peaks between total wavenumbers 10 and 20 (Hartmann et al. 1995).

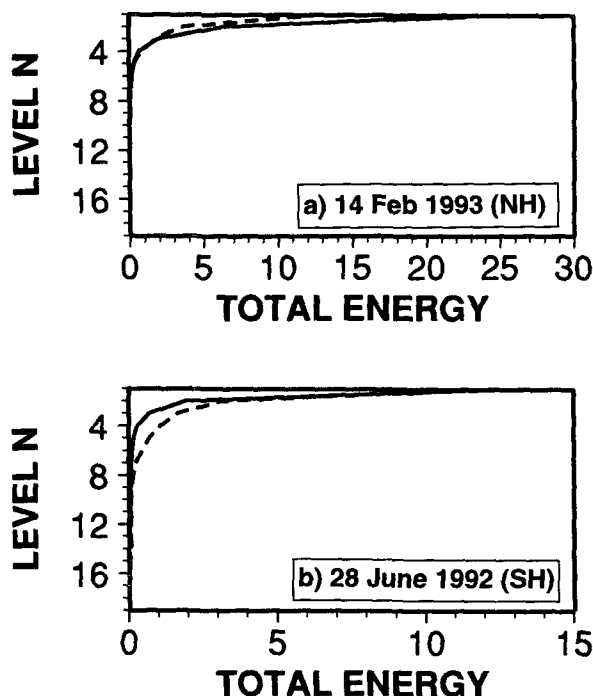


FIG. 1. Total singular vector perturbation energy as a function of model level averaged for the first six singular vectors for the two cases of 14 February 1993 in the NH and 28 June 1992 in the SH. The initial energy is multiplied by a factor of 20 to be visible and is represented by a dashed line. The final energy is shown by a solid line.

The basic streamfunction fields at the top model level at the initial time are shown in Fig. 3 for the same cases of interest as in Fig. 2. The rapidly growing disturbances are associated with a highly distorted polar vortex that results in strong localized jet structures bounded by regions of less intense wind (Figs. 3a–c). The occasions of very weak growth are associated with a very weak vortex (Fig. 3d) or with the strong but very symmetric vortex of the Southern Hemisphere. The case in which the SH vortex is more distorted (Fig. 3f) gives more rapid growth than the case in which it is nearly zonally symmetric (Fig. 3e).

Figure 4 shows the initial and final streamfunction perturbations at the top model level that are associated with the first singular vector for three of the six cases shown in Figs. 2 and 3. In each case the initial perturbation is in the weaker winds upstream and equatorward of a localized jet structure, and the final energy is maximized when the disturbance has propagated downstream and poleward to reach the core of the jet. These characteristics are consistent with growth through the meridional shear and east–west variation of the basic flow and are consistent with wave action concepts that indicate the wave energy should increase as the wave propagates into regions of larger Doppler-shifted frequency (Bretherton and Garrett 1968; Zeng

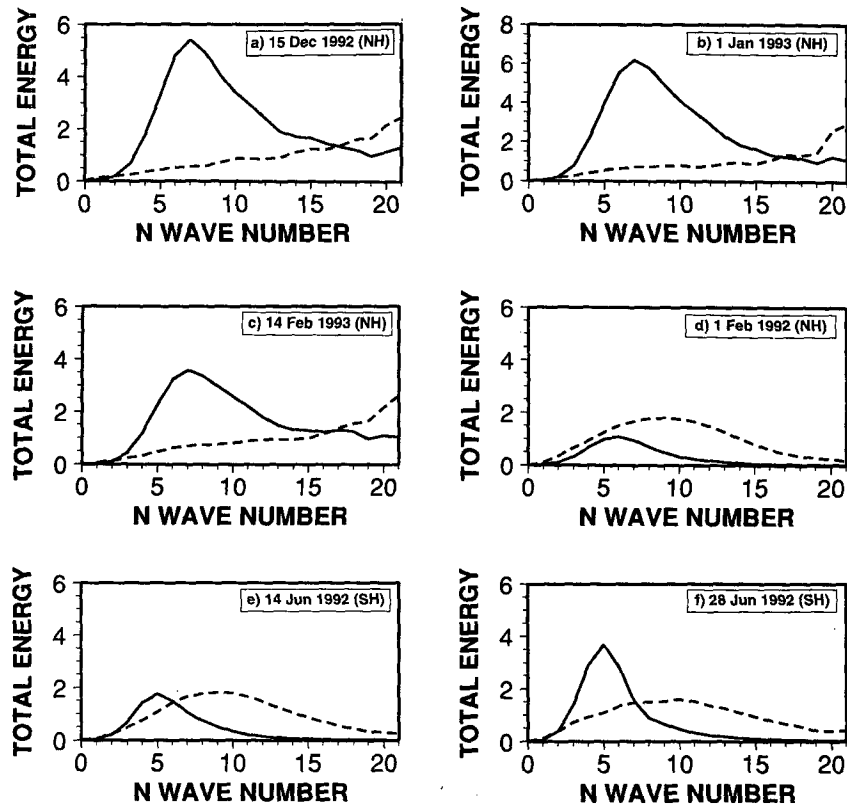


FIG. 2. Total singular vector perturbation energy as a function of total spherical harmonic wavenumber averaged over the first six singular vectors at initial (dashed) and final (solid) time for each of six wintertime cases of interest: (a) 15 December 1992 in NH, (b) 1 January 1993 in NH, (c) 14 February 1993 in NH, (d) 1 February 1992 in NH, (e) 14 June 1992 in SH, and (f) 28 June 1992 in SH. The initial energy is multiplied by a factor of 20 to be visible on the same plot with the final energy.

1983; Buizza and Palmer 1995). For the cases shown in Fig. 4, each dominant singular vector is accompanied by another singular vector with a slightly smaller growth rate and a structure whose phase is approximately in quadrature with the dominant singular vector. Most singular vectors on the main polar vortex thus come in conjugate pairs. Vertical propagation seems to play a relatively modest role in the growth of the disturbances. The singular vectors show almost no tilt with height at both initial and final times, and the vertical structure of the perturbation energy has a similar shape at both initial and final times. Singular vector calculations from a model with a higher model top and more vertical resolution in the stratosphere are presented below in order to investigate the role of the top boundary in the structure of the modes.

Beginning with the case of 1 January 1993 (base streamfunction in Fig. 3b and singular vector structure in Figs. 4a,b), we see that the first singular vector has an initial structure centered at about 35°N along a range of longitudes from about 90° to 40°W . This places it on the outer edge of the vortex, upstream of the region

of strong winds (as evidenced by strong streamfunction gradients in Fig. 3) that is considerably farther poleward and downstream of the initial position of the dominant singular vector. In 48 hours the singular vector propagates through about 90° of longitude to 45°E and poleward to about 60°N while increasing its amplitude by about a factor of 10.

A similar development occurs for the dominant singular vector on 14 February 1993, except that in this case the vortex is more displaced off the pole and a strong jet extends directly over the pole from 90°E to 90°W . At initial time the singular vector energy is located in the weaker winds of midlatitudes between about 0° and 45°E , where it is tilted against the shear (Fig. 4c). At final time the singular vector appears as a wave train aligned with the jet crossing the pole (Fig. 4d).

Singular vectors for the more zonal flow of the Southern Hemisphere are larger in scale both at initial and final time. For the more zonally symmetric flow the singular vectors become nearly zonally periodic wave trains with zonal wavenumber 2 or 3 (not

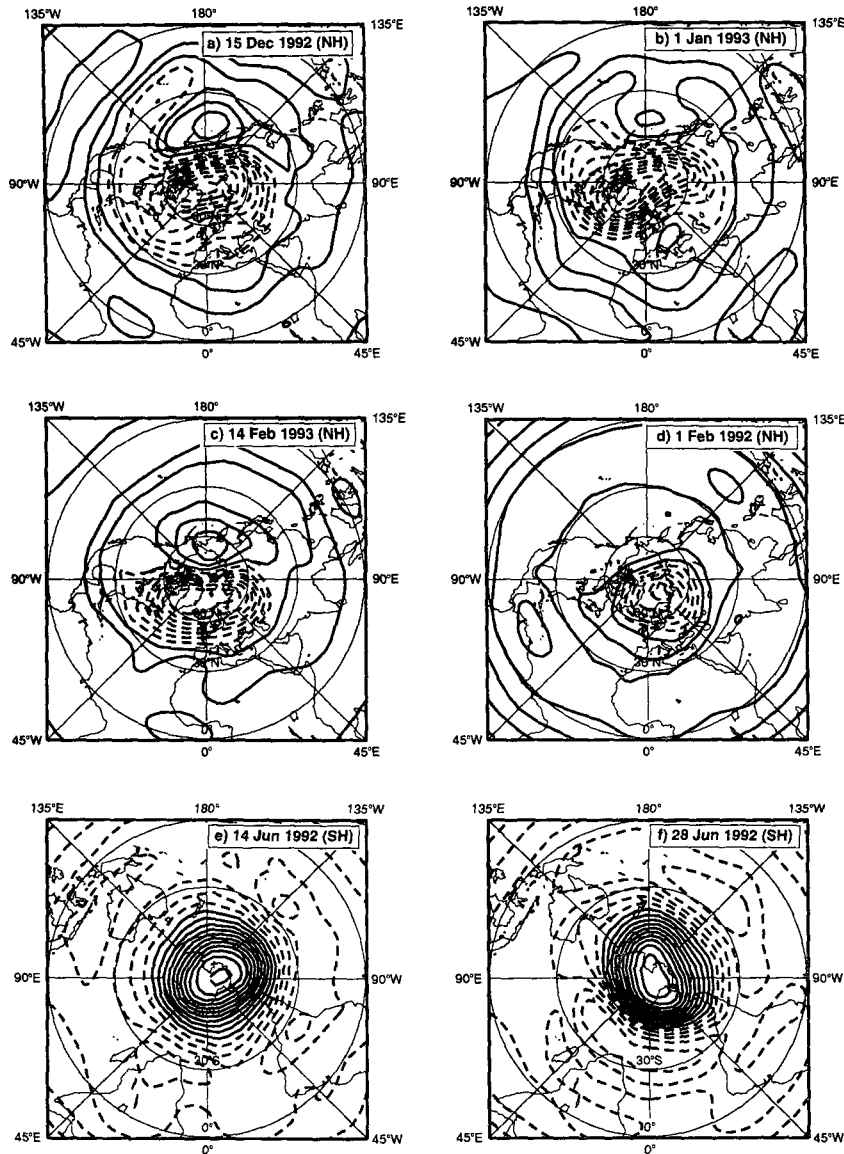


FIG. 3. Basic streamfunction field at initial time at the top model level for the six cases shown in Fig. 2. Negative streamfunction values are dashed. Contour interval is 20 in all plots.

shown). In the more perturbed case of 28 June 1992 the singular vectors are more localized to take advantage of the stronger winds poleward of Africa at about 30°E (Fig. 3f). The singular vector is initially located in the rather weak winds outside the vortex, slightly to the west (upstream) of where the maximum mean winds are located.¹ Its structure is very zonally elongated, with some northeast–southwest tilt of the more

upstream of the three anomaly centers. The structure appears to grow through meridional propagation into the stronger eastward winds of the polar vortex. Downstream energy propagation also seems important, but very little zonal phase propagation is observed. The distinction between phase propagation and energy propagation will be more visible when daily 10-mb maps are considered in the next section. The growing disturbances appear to be quasi-stationary despite the strong mean eastward wind speed in the jets. Small phase speeds were also a characteristic of the modal instabilities of zonally asymmetric stratospheric flows presented by Frederiksen (1982). This low phase speed

¹ Remember that eastward flow is clockwise in a Southern Hemisphere polar stereographic projection and counterclockwise in a Northern Hemisphere polar stereographic projection.

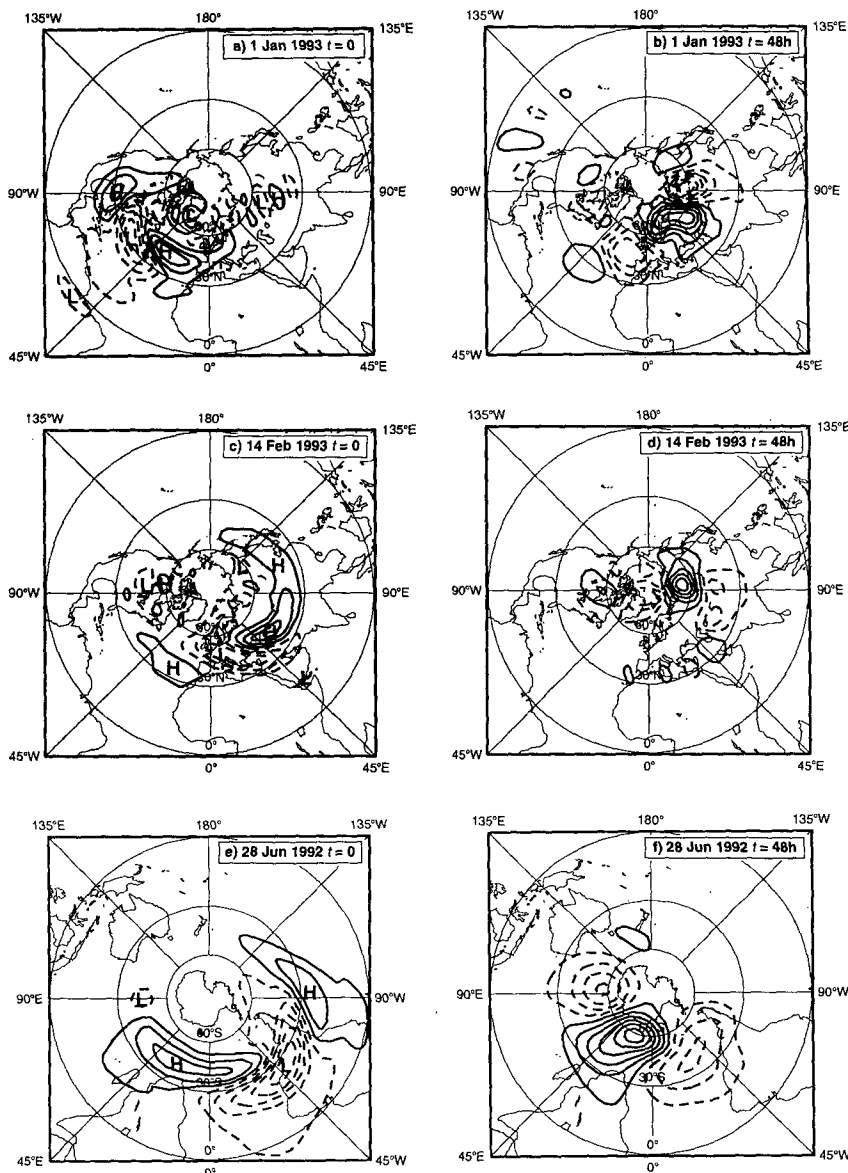


FIG. 4. Streamfunction perturbations associated with the first singular vector at the top model level at initial time (left) and final time (right): (a), (b) 1 January 1993 in NH; (c), (d) 14 February 1993 in NH; and (e), (f) 28 June 1992 in SH. The contour interval in the NH (SH) cases is ten (20/3) times as big for the final time as for the initial time.

may be required so that the perturbations can remain in the optimal growth region during the period of growth. This in turn gives rise to the rather large spatial scales required to remain stationary in the presence of strong zonal winds (e.g., Hoskins and Karoly 1981).

When the vortex develops an equatorward arm of jet structure such as the one extending from California toward Hawaii in the 15 December 1992 case in Fig. 3a, secondary growing structures on this arm are possible. McIntyre and Palmer (1984) suggested that instabilities of the associated arm of high potential vorticity air

might be responsible for more effective mixing within the "surf zone" outside the main vortex. Dritschel (1989) and Dritschel et al. (1991) have shown, however, that adverse shear and strain of adequate magnitude can stabilize shear instabilities of this type. The extended trough in this case has an eastward jet on its equatorward flank in the Tropics and a westward jet on its northward flank adjacent to the high pressure center in the mid-Pacific. The potential vorticity structure on the 500 K theta surface on 15 December 1992 is shown in Fig. 5. The 24-h forecast from the ECMWF model

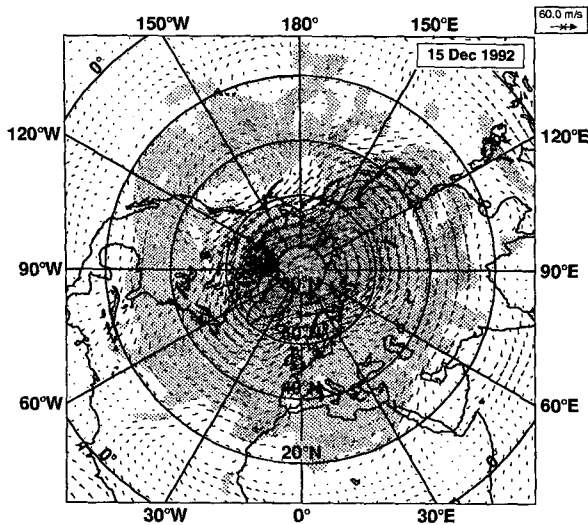


FIG. 5. Polar stereographic projection of the wind vectors and potential vorticity distribution on the 500 K theta surface on 15 December 1992. Potential vorticity values greater than $2 \times 10^{-6} \text{ m}^2 \text{ s}^{-1} \text{ K kg}^{-1}$ are shaded.

is shown at T106 resolution in order to reduce noise associated with the initial analysis. An arm of high potential vorticity air and associated reverse flow can be seen west of North America over the Pacific Ocean, although it is somewhat diffuse at this level.

To resolve these structures better, T42 singular vector calculations have been done for the 15 December 1992 case.² Figure 6 shows the first and third singular vector for the case of 15 December 1992. The first singular vector (Figs. 6a,b) and its associated conjugate,³ which is the second singular vector (not shown), are similar to the main vortex singular vectors previously discussed. The third singular vector and its conjugate are located in the protruding arm of the vortex and are associated with the shears and vorticity gradients there. Much of the initial energy of the third singular vector (Fig. 6c) is located at the base of the arm where it meets the main vortex, but significant initial energy also appears at the westward end of the tropical eastward jet portion of the arm. Much of the initial amplitude is located in the regions of weak wind in the center of the extended trough. The singular vector structure at final time is of fairly large horizontal scale and represents a wavelike disturbance along the extended trough (Fig. 6d). That the second pair of singular vectors appears

to be associated solely with the extended trough supports the notion of McIntyre and Palmer (1984) that these armlike extensions of the main vortex are regions where disturbances can grow efficiently. It is reasonable to postulate that these disturbances may be helpful in mixing the high potential vorticity air in the arm with the generally lower potential vorticity air outside the vortex.

The vertical energy structure in Fig. 1 suggests a very strong influence of the upper boundary. To provide evidence that the singular vector structures are not wholly dependent on the presence of the upper boundary, we have performed some singular vector calculations with a T42L25 version of the model. In this version six more levels were added above 100 mb, and the top level was moved from 10 to 3.5 mb. The top was not moved higher than 3.5 mb because we feared the result would then be strongly affected by the extrapolation of the analysis above the levels where data are available. The stratospheric levels for the L25 and L19 versions are shown in Table 1. These calculations were done with a later revision of the ECMWF model than those shown in Fig. 1, so we have also done a new T42L19 singular vector calculation to make the comparison as precise as possible. For the T42L25 case the energy growth was optimized for the top nine layers, which correspond to approximately the same mass of the atmosphere as the top three layers in the T42L19 case.

Figure 7 shows the vertical and spectral structure of the total energy averaged over the first eight singular vectors for the T42L25 and T42L19 experiments for 15 December 1992. In the T42L19 case both the initial and final energy are peaked strongly near the model top. The T42 calculation seems to resolve very well the growing structures since the initial energy spectrum becomes quite small for the highest total wavenumbers included in the T42 calculation. The final energy again peaks near total wavenumber 6 or 7. In this respect the stratosphere is different from the troposphere, where significant growth can be initiated from spatial scales considerably smaller than that of total wavenumber 42, and even in T42 calculations the energy spectrum of the initial perturbation shows no evidence of declining at total wavenumber 42 (Hartmann et al. 1995). T42 resolution is apparently not required to obtain the structures discussed here since the resulting structures appear very similar to those obtained for the same case using T21 resolution (not shown).

In the 25-level case the initial and final energies increase slowly with height between layers 9 and 2 but increase abruptly for the top layer. This suggests that a major part of the effect of the top boundary is confined to the topmost level of the model. This is not at all obvious in the 19-level case, in which the stratospheric resolution is too poor to distinguish the internal structure from the boundary effect. Figure 8 shows the vertical structure of the initial and final energies for the

² The equatorward latitude of the domain of final energy optimization was inadvertently shifted from the equator to 10°N in this calculation, but this does not appear to have made a significant difference in the resulting structure.

³ The conjugate pairs of singular vectors have a similar location and structure to each other but are shifted by one-quarter of an effective wavelength so as to be spatially orthogonal.

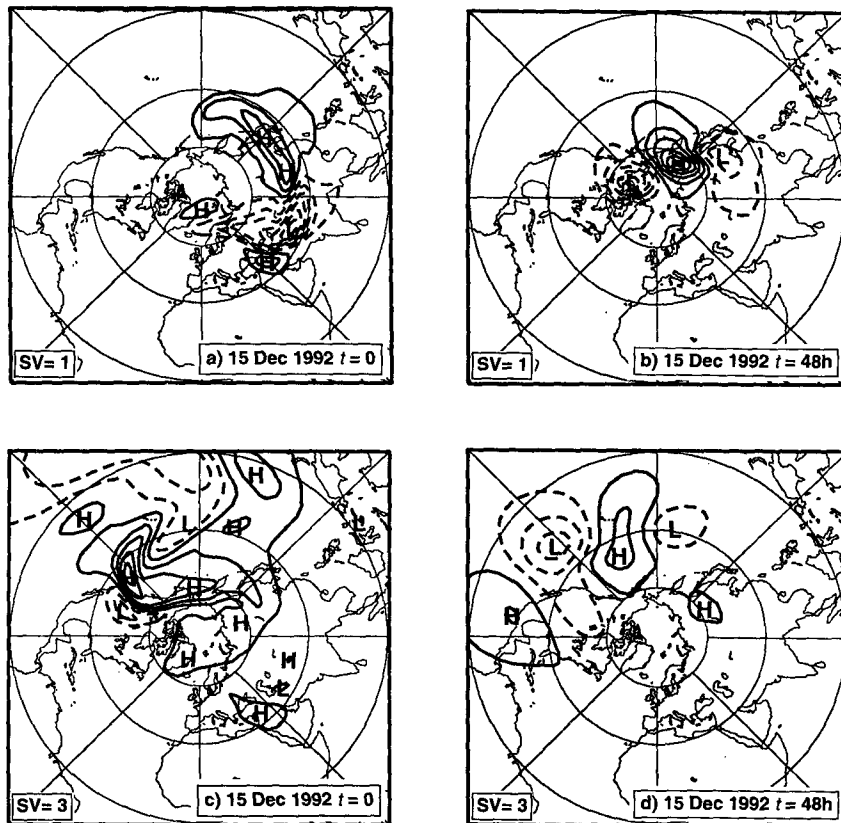


FIG. 6. As in Fig. 4 except for the first and third singular vectors (SV) of the 15 December 1992 case in the NH calculated at T42. Contour interval for final time perturbation (on right) is 10 times that of initial time perturbation.

first, third, fifth, and seventh singular vectors of the T42L25 case. Some show maximum energy near the top, while others have a broad maximum in the lower stratosphere below the top. All show an increase at the top level that must be an artifact of the model top.

The horizontal structures of the first two modes are very similar in the T42L25 and T42L19 cases (Fig. 9). The mode that grows along the protruding arm of the vortex for the 15 December 1992 case also appears in the T42L25 calculation, but as mode 5 rather than mode 3 as shown previously. If one looks carefully at the singular value spectrum for this case, the first two modes have singular values about twice those of the third and fourth, but the separation between singular values of succeeding modes is much less. So the ordering of singular vectors three through eight can be shifted around rather easily, though their structures seem to maintain their identity through the geographical locations of their major features.

Overall, we conclude that despite the presence of the model top in the middle of the stratosphere, the horizontal structure and location of the singular vectors are not terribly sensitive to the position of the top nor to the resolution in the stratosphere. This is consistent

with the results of Simmons and Strüfing (1983), who found that a model with similar vertical resolution (18 levels and top at 10 mb) did a very reasonable job of forecasting stratospheric warmings.

4. Nonlinear evolution of singular vector perturbations

In this section we investigate the evolution of the singular vector perturbations when they are added to the initial conditions in integrations of a T63L19 full-physics version of the ECMWF model. The singular vectors are linear structures and have no specific amplitude, so an amplitude must be given before they can be added to the analysis. The amplitude of the perturbation is chosen to be smaller than the expected error in the analysis and yet large enough so that the perturbations become nonlinear after a few days. The fields are then reinitialized and a new forecast is made with the perturbed initial condition. It happens that these perturbations can trigger important nonlinear interactions with the vortex, particularly if they augment existing asymmetries in the vortex structure.

Figure 10 shows a sequence of 10-mb maps for forecasts initialized on 14 February 1993. The first column

TABLE 1. Stratospheric pressure levels in the 25-level and 19-level calculations.

25 level		19 level	
Level number	Pressure	Level number	Pressure
1	3.5	—	—
2	8.5	—	—
3	12.5	1	10.0
4	18.0	—	—
5	24.5	—	—
6	31.5	2	30.0
7	38.5	—	—
8	46.0	3	50.4
9	55.4	—	—
10	73.4	4	73.4
11	102.7	5	102.7
12	141.2	6	141.2

shows the control forecast over a period of four days. The second column shows a forecast perturbed with the first singular vector previously shown in Fig. 4c, except with opposite sign. The difference between the perturbed forecast and the control is shown in column 3. Column 4 shows the difference between a perturbed forecast and the control when the perturbation is given the same amplitude but opposite sign to that shown in column 3. Early in the forecast the last two columns show difference fields that are identical in shape but opposite in sign, but as time goes on significant nonlinear effects can be seen. In particular, with the sign chosen for the third column, rather significant changes occur, and something approaching a minor warming is induced from relatively small initial perturbations. The maximum 10-mb height perturbation on day zero is about 125 m, but this leads to the vortex nearly break-

ing into two pieces with height perturbations as large as 900 m on day 4. It is clear that nonlinear effects are necessary to effect this large perturbation of the vortex, because if the same perturbation is applied with opposite sign, as in the last column of Fig. 10, then the vortex is only slightly disturbed (not shown), and the height anomalies on day 4 are reduced to about 450 m (last map in the fourth column of Fig. 10). A simple observation that can be made about this difference is that the sign used in column three results in a more asymmetric vortex at day 2. The vortex is initially off the pole and elongated along the direction of the 90°E–90°W meridian, and the addition of the perturbation exacerbates this elongation and introduces a bend in the middle that threatens to break off a piece of the vortex. On the other hand, the same perturbation with the sign used in column 4 tends to reduce the existing asymmetry of the vortex and ultimately has a much smaller effect on its evolution.

Somewhat surprisingly, an even stronger sensitivity to the sign of the perturbation is found for the case of 28 June 1992 in the Southern Hemisphere (Fig. 11). Despite the fact that the polar vortex is relatively intense and symmetric looking, there is a quite strong localized jet poleward of Africa. Height perturbations of about 75 m around the vortex can lead to quite significant differences in the vortex shape at later times, if the perturbations are of the right polarity to interact strongly with the existing asymmetry of the vortex. For the sign of the perturbation given in column 3 of Fig. 11, the vortex shape is significantly changed and height perturbations on day 4 exceed 1350 m. These large differences persist through a full 10 day forecast (not shown). For the opposite sign of the initial perturbation (column 4 of Fig. 11) the height perturbations on day 4 are only about 300 m and declining.

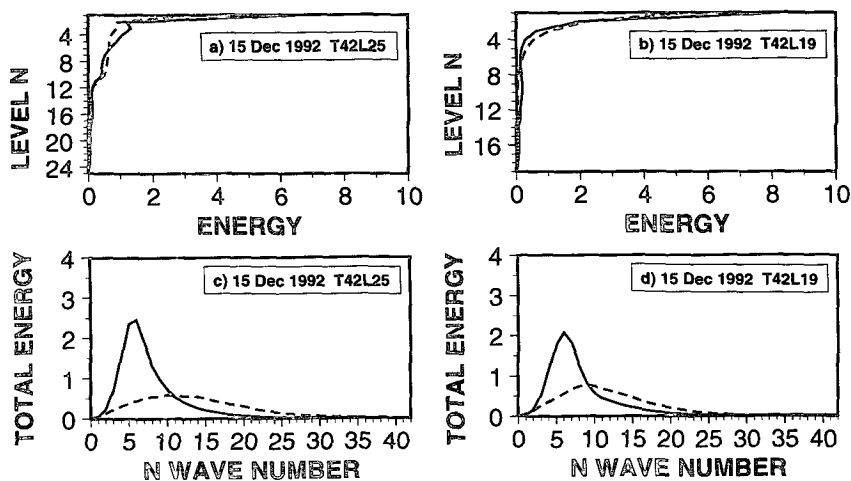


FIG. 7. Initial (dashed) and final (solid) vertical and spectral energy distributions, averaged for the first eight singular vectors of the 15 December 1992 case for (a), (c) T42L25 case and (b), (d) T42L19 case. Initial energies have been multiplied by 10.

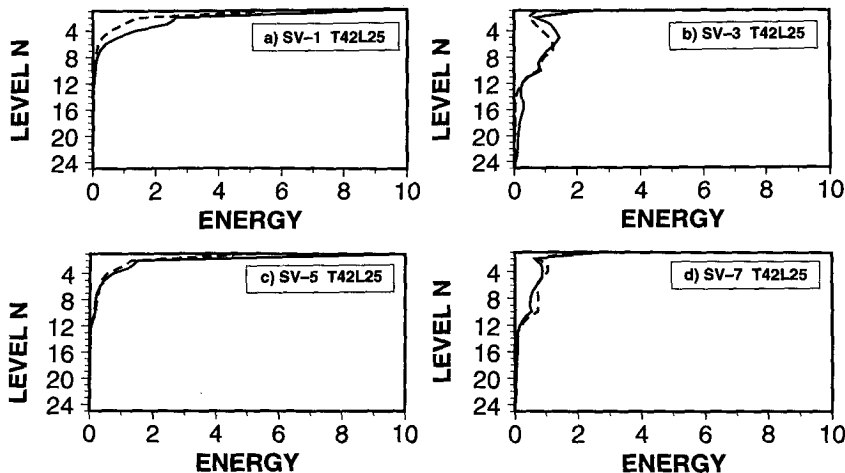


FIG. 8. Initial and final vertical energy distributions for the (a) first, (b) third, (c) fifth, and (d) seventh singular vectors of the T42L25 calculation for 15 December 1992.

Perturbations that grow along the armlike protrusions of the polar vortex appear to propagate away from the main vortex and have relatively weak interactions

with it. Figure 12 shows a series of 10-mb maps for the 15 December 1992 case perturbed with both signs of the third singular vector shown previously in Figs. 6c

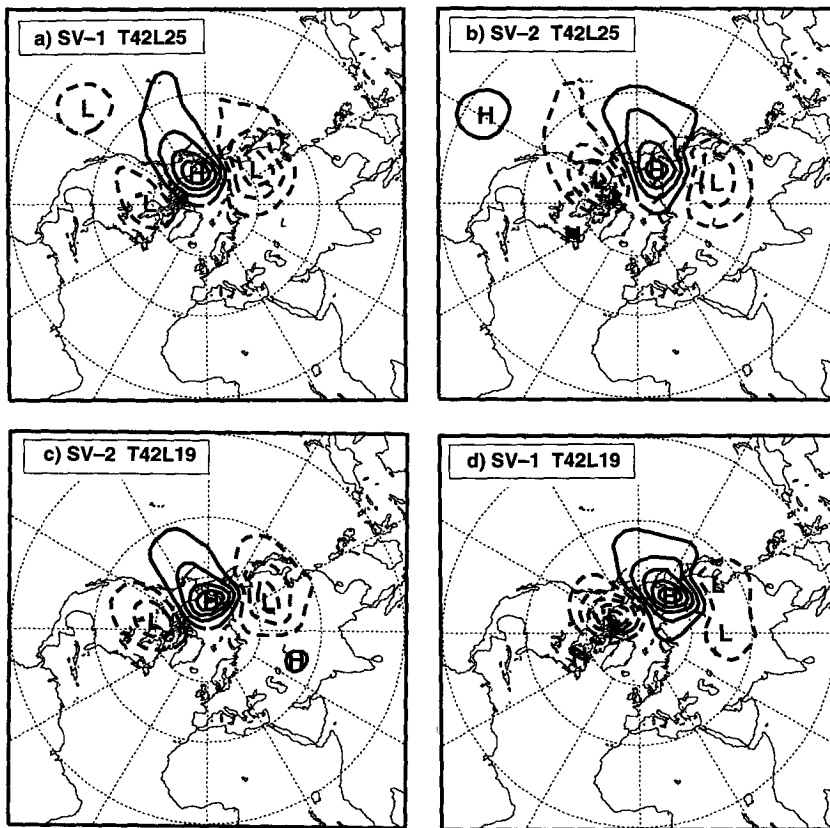


FIG. 9. Final-time (48 h) singular vector streamfunctions for the 15 December 1992 case: (a) SV-1, (b) SV-2 for the T42L25 case at level 2 (8.5 mb), (c) SV-2, and (d) SV-1 for the T42L19 case at level 1 (10 mb).

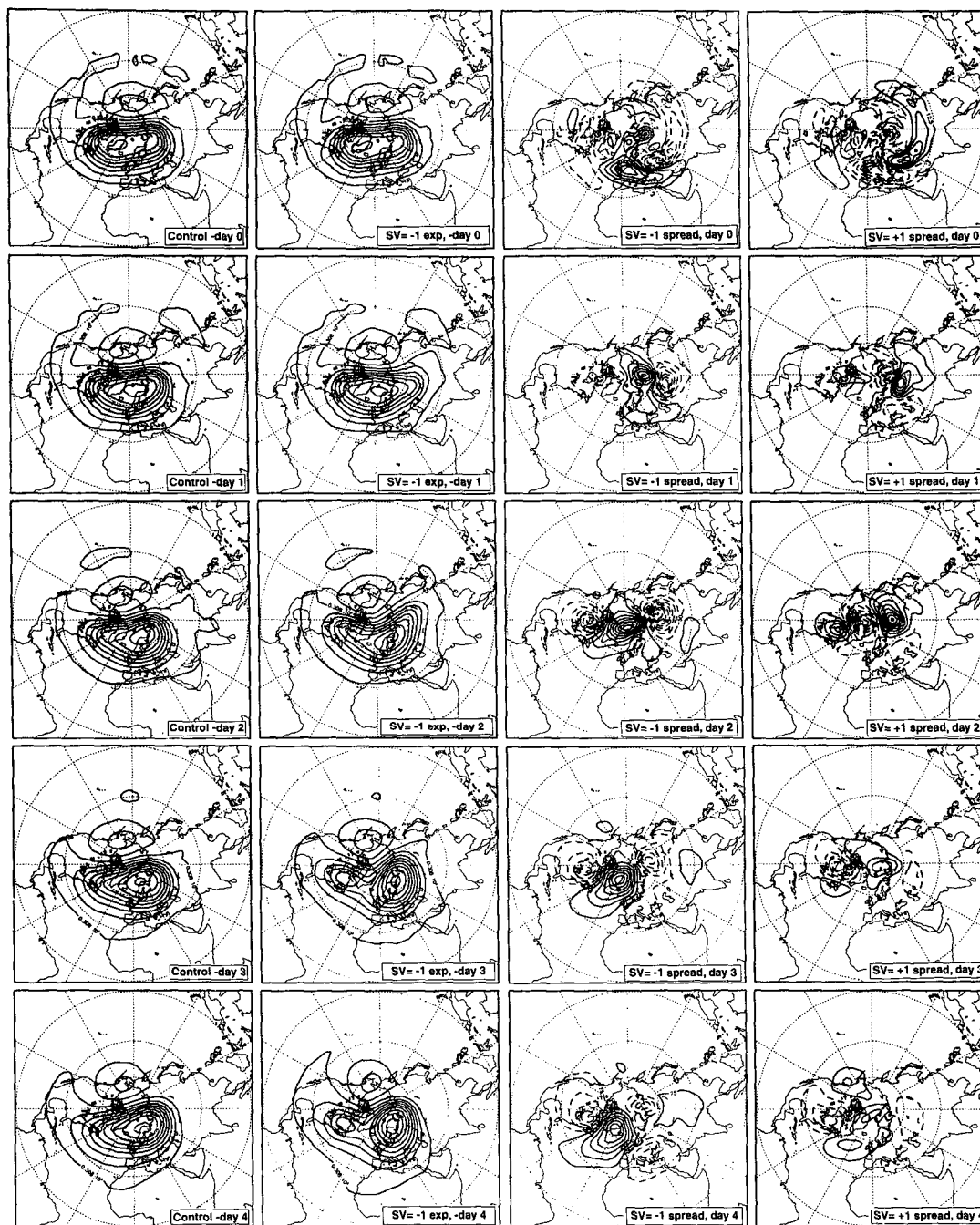


FIG. 10. Northern Hemisphere polar stereographic maps of height of the 10-mb surface at 1-day intervals for T63 forecasts starting on 14 February 1993. The initial analysis is shown at the top and subsequent days are placed below, ending with the 4-day forecast on the bottom. The first column gives the control forecast; the second column gives the forecast perturbed with the first singular vector shown in Fig. 4c except with opposite sign; the third column shows the difference between the perturbed forecast in column two and the control forecast in column one, and the fourth column shows the difference between a perturbed forecast and the control when the perturbation is given the same amplitude but opposite sign. For the first and second columns the contour interval is 300 m; for the third and fourth columns the contour interval is 25 m for the analysis ($t = 0$), 100 m for the 1-day and 2-day forecasts ($t = 1$ and $t = 2$), and 150 m for the 3-day and 4-day forecasts ($t = 3$ and $t = 4$). The zero contour is straddled, so that the lowest positive contour levels are 12.5, 50, and 75 m.

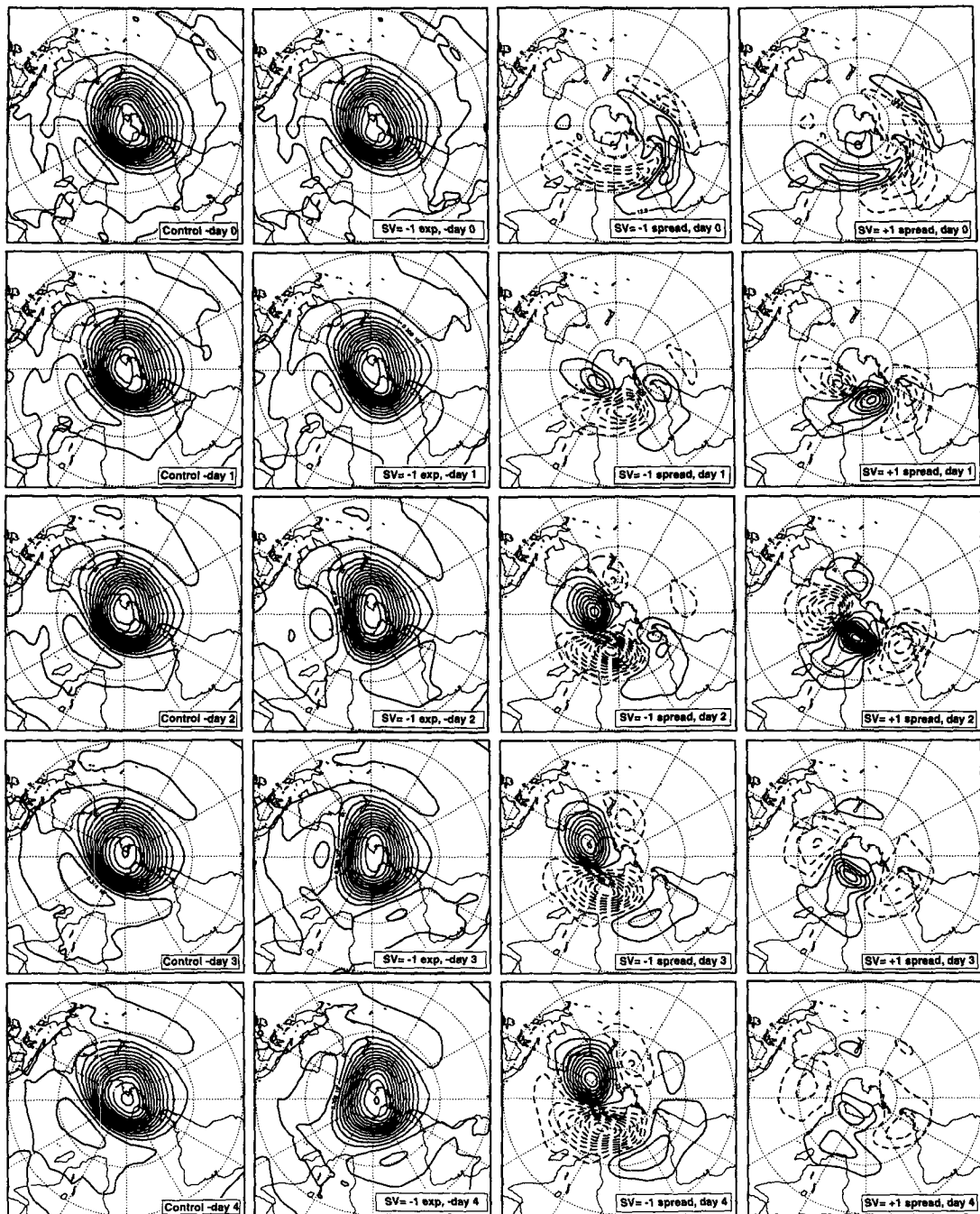


FIG. 11. Southern Hemisphere polar stereographic maps of height of the 10-mb surface at 1-day intervals for T63 forecasts starting on 28 June 1992. The arrangement is as in Fig. 10, except as noted here. The second column gives the forecast perturbed with the first singular vector as shown in Fig. 4e except with opposite sign, the third column shows the difference between this perturbed forecast and the control forecast in column one, and the final column shows the difference between a perturbed forecast with the opposite sign as in column 3 and the control forecast. The contour intervals are as for Fig. 10.

and 6d. The height perturbations are initially concentrated near the point where the equatorward extension is attached to the main vortex, and they propagate slowly westward and equatorward with time. Their

scale is rather large and their movements slow, so that one would expect to be able to capture this form of wave activity with satellite measurements in the middle and upper stratosphere. For the amplitude chosen in this

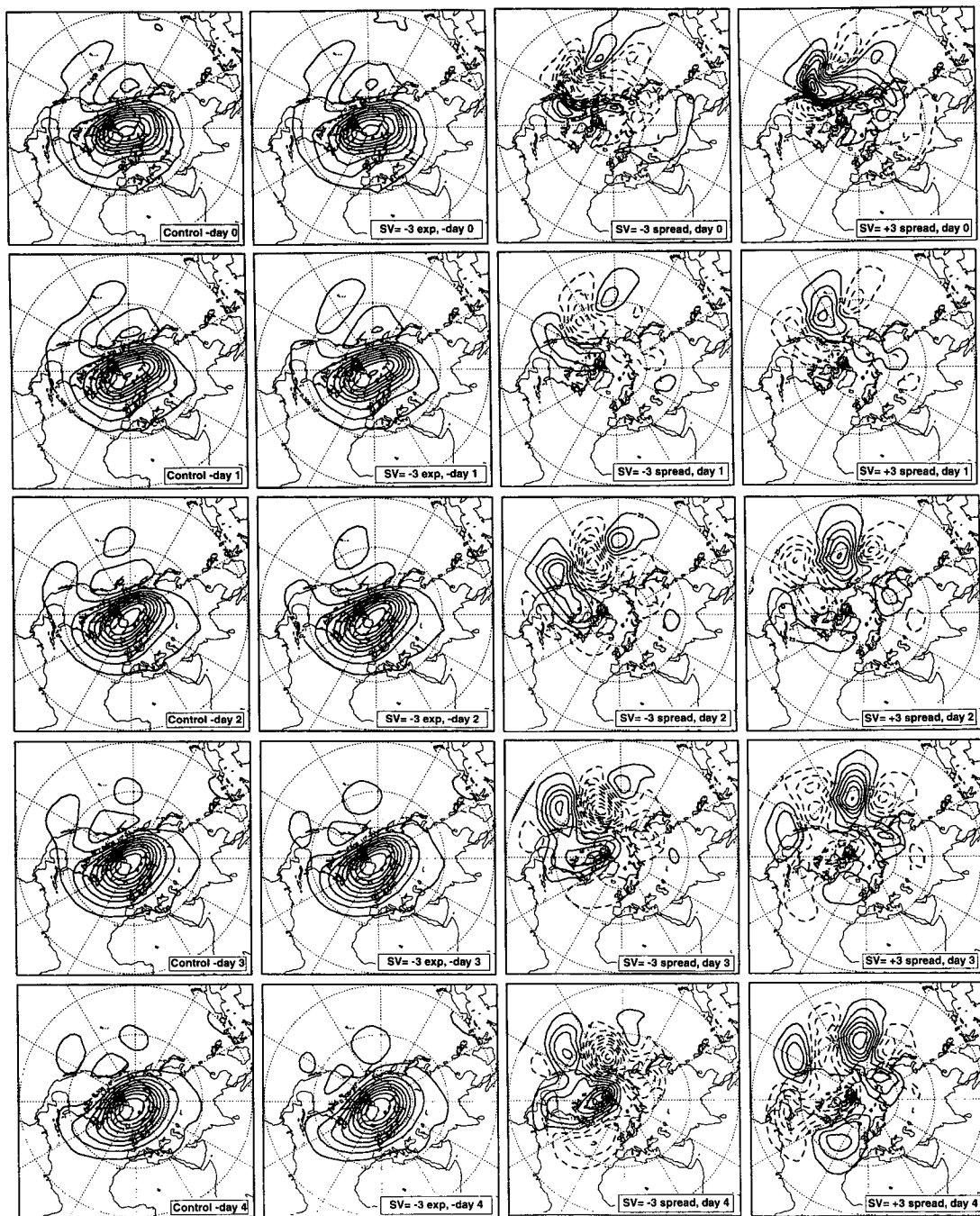


FIG. 12. Northern Hemisphere polar stereographic maps of height of the 10-mb surface at 1-day intervals for T63 forecasts starting on 15 December 1992. The arrangement is as in Fig. 10, except as noted here. The second column gives the forecast perturbed with the third singular vector shown in Fig. 6c except with opposite sign, and the final column shows the difference between a perturbed forecast with the third singular vector with the same sign as occurs in Fig. 6c and the control forecast. For the third and fourth columns the contour interval is 10 m for the analysis ($t = 0$), and 50 m for all subsequent times. The zero contour is straddled, so that the lowest positive contour levels for the difference plots are 5 and 25 m.

example, some modest nonlinearities appear around day 3 or 4. In particular, the low center originally off the coast of North America in the third column of Fig.

12 shows more development and less of a tendency to propagate away from the main vortex than the corresponding high center in column four. The perturbations

appear to hasten the demise of the protrusion, but the effect is not dramatic because the protrusion weakens rapidly, even in the control forecast. The control forecast seems already to contain perturbations on the arm of similar scale and structure to the singular vectors. If the singular vectors are indeed some of the fastest-growing disturbances, then it should not be surprising to occasionally find them in a control forecast initialized from the observed state.

5. Conclusions

In this paper we have attempted a preliminary exploration of the finite-time instabilities or singular vectors of lower stratospheric flow as captured in T21 and T42 versions of the 19-level ECMWF prediction model. Structures that increase their energy by factors of 20 or more in 48 hours are identified. They are primarily of large horizontal scale, both at their initial and final times. The energy of the initial perturbation is spread across a broad range of spatial scales centered in the vicinity of total spherical harmonic wavenumbers 10 to 15, but the energy spectrum 48 hours later is more sharply peaked near total wavenumber 5 to 7. The scale depends somewhat on the structure of the mean state. Mean states showing stronger jet structures give stronger singular vector growth, and the singular vectors for these more asymmetric states have smaller scales at both initial and final time.

Perturbations that grow on the main stratospheric vortex begin as zonally elongated wavetrains tilted against the shear and located equatorward and upstream of the strongest localized jet structure associated with the vortex. At final time the disturbances appear as wave trains in the jet structures themselves. Asymmetric vortices with stronger localized jet structures in the base state appear to foster more rapidly growing singular vectors than more zonally symmetric vortices. Greater wave growth on more asymmetric vortices is consistent with the modal instability calculations of Frederiksen (1982). The relative importance of zonal and meridional propagation during the growth period depends on the basic vortex structure. For vortices displaced significantly off the pole, as is often observed in the Northern Hemisphere, zonal energy propagation seems to be very important. For the vortex structure more typically observed in midwinter in the Southern Hemisphere, meridional energy propagation with relatively little zonal phase propagation seems to characterize the dominant singular vector.

When the polar vortex is distorted and a large arm of vortex air is peeled off and extended into lower latitudes (e.g., McIntyre and Palmer 1983), the extension of the vortex toward the Tropics provides a feature on which disturbances can efficiently grow. In the 15 December 1992 case investigated here, a pair of the dominant singular vectors were associated with the extension of the vortex and its associated jet structure. The

structures that grow on the extension from the vortex originate near where the tropical extension is attached to the main vortex and then propagate equatorward along the extension toward the Tropics. For the amplitudes chosen here the structures that grow along the arm of the vortex appear to have relatively weak interactions with the main vortex. These growing disturbances appear to assist in the breakup of the arm of vortex air and its mixing with the air outside the vortex. This evidence is consistent with suggestions by McIntyre and Palmer (1984) that arms of high potential vorticity air extruded from the main vortex would support wave growth and that waves developing on the arms would assist in their breakup.

Singular vector perturbations of the main vortex appear to stimulate nonlinear interactions with the vortex that result in significant changes in its shape and evolution. These nonlinear interactions are most effective where the vortex has some preexisting asymmetry, and it is at these times that the linear growth rates of the singular vectors are also greatest. One can conjecture that at these times the predictability of stratospheric flow is most sensitive to errors in the stratospheric analysis. These arguments are consistent with prior suggestions that the stratospheric polar vortex must be "preconditioned" before upward-propagating planetary waves can induce a major stratospheric warming (e.g., McIntyre 1982). The difference is that we are considering the effect of small disturbances already in the stratosphere, and the changes they can induce are usually changes in the shape of the vortex, or at most minor warmings. The spatial scale of the singular vector perturbations at initial time are generally smaller than the scale of waves that can most easily propagate upward from the troposphere.

Finally, it must be mentioned again that to every result shown here must be attached the caveat that the action of interest is so near the model top. We have shown that moving the top up a little does not change the horizontal structure of the dominant singular vectors, and we argue that much of what we see is probably relevant to an effectively unbounded atmosphere, but this must be verified by actual computation at some future time. The growth mechanisms are mostly associated with lateral propagation from regions of weak wind to regions of strong wind. Such growth mechanisms are also observed in the troposphere where the model top is not a serious constraint (e.g., Buizza and Palmer 1995). The spatial scales that are best able to take advantage of the lateral shear in the lower stratosphere are not the spatial scales with the most efficient vertical propagation (e.g., total wavenumbers 5–7). Therefore, we argue hopefully that while these results are certainly relevant in the context of the ECMWF model, which has its top level near 10 mb, they may also be of more general relevance to understanding the dynamics of the stratosphere.

Acknowledgments. The existence of significant singular vector growth in the stratosphere was first brought to our attention by Dr. Robert Mureau. We were motivated to continue this work by discussions with Dr. E. Kalnay. Professor J. R. Holton provided useful comments on an early draft of this paper. Candace Gudmundson edited the manuscript and Kay Dewar provided graphics assistance. This work was conducted while DLH was a visitor at ECMWF. Additional support for DLH was provided by the Climate Dynamics Program of the National Science Foundation under Grant ATM 9313383.

REFERENCES

- Andrews, D. G., J. R. Holton, and C. B. Leovy, 1987: *Middle Atmosphere Dynamics*. Academic Press, 489 pp.
- Borges, M. D., and D. L. Hartmann, 1992: Barotropic instability and optimal perturbations of observed nonzonal flows. *J. Atmos. Sci.*, **49**, 335–354.
- Bretherton, F. P., and C. J. R. Garrett, 1968: Wavetrains in inhomogeneous moving media. *Proc. Roy. Soc. London*, **A302**, 529–554.
- Buizza, R., 1994: Sensitivity of optimal unstable structures. *Quart. J. Roy. Meteor. Soc.*, **120**, 429–451.
- , and T. N. Palmer, 1995: The singular-vector structure of the atmospheric general circulation. *J. Atmos. Sci.*, **52**, 1434–1456.
- , J. Tribbia, F. Molteni, and T. Palmer, 1993: Computation of optimal unstable structures for a numerical weather prediction model. *Tellus*, **45A**, 388–407.
- Dritschel, D. G., 1989: On the stabilization of a two-dimensional vortex strip by adverse shear. *J. Fluid Mech.*, **206**, 193–221.
- , P. H. Haynes, M. N. Jukes, and T. G. Shepherd, 1991: The stability of a two-dimensional vorticity filament under uniform strain. *J. Fluid Mech.*, **230**, 647–665.
- Farrell, B. F., 1982: The initial growth of disturbances in a baroclinic flow. *J. Atmos. Sci.*, **39**, 1663–1686.
- , 1989: Optimal excitation of baroclinic waves. *J. Atmos. Sci.*, **46**, 1193–1206.
- , and P. J. Ioannou, 1994: A theory for the statistical equilibrium energy spectrum and heat flux produced by transient baroclinic waves. *J. Atmos. Sci.*, **51**, 2685–2698.
- Frederiksen, J. S., 1982: Instability of the three-dimensional distorted stratospheric polar vortex at the onset of the sudden warming. *J. Atmos. Sci.*, **39**, 2313–2329.
- Hartmann, D. L., 1983: Barotropic instability of the polar night jet stream. *J. Atmos. Sci.*, **40**, 817–835.
- , 1985: Some aspects of stratospheric dynamics. *Issues in Atmospheric and Oceanic Modeling; Part A Climate Dynamics*, S. Manabe, Ed., Academic Press, 219–247.
- , R. Buizza, and T. N. Palmer, 1995: Singular vectors: The effect of spatial scale on linear growth of disturbances. *J. Atmos. Sci.*, **52**, 3885–3894.
- Hoskins, B. J., and D. J. Karoly, 1981: The steady-state linear response of a spherical atmosphere to thermal and orographic forcing. *J. Atmos. Sci.*, **38**, 1179–1196.
- Ishioka, K., and S. Yoden, 1994: Nonlinear evolution of a barotropically unstable circumpolar vortex. *J. Meteor. Soc. Japan*, **72**, 63–80.
- Kalnay, E., and Z. Toth, 1995: The breeding method. *Proc. ECMWF Seminar on Predictability*, Reading, United Kingdom, European Centre for Medium Range Weather Forecasts, 59–68. [Available from ECMWF, Shinfield Park, Reading, U.K. RG2 9AX.]
- Lacarra, J.-F., and O. Talagrand, 1988: Short-range evolution of small perturbations in a barotropic model. *Tellus*, **17**, 321–333.
- Manney, G. L., C. R. Mechoso, L. S. Elson, and J. D. Farrara, 1991: Planetary-scale waves in the Southern Hemisphere winter and early spring stratosphere: Stability analysis. *J. Atmos. Sci.*, **48**, 2509–2523.
- McIntyre, M. E., 1982: How well do we understand the dynamics of stratospheric warmings? *J. Meteor. Soc. Japan*, **60**, 37–65.
- , and T. N. Palmer, 1983: Breaking planetary waves in the stratosphere. *Nature*, **305**, 593–600.
- , and —, 1984: The “surf zone” in the stratosphere. *J. Atmos. Terr. Phys.*, **46**, 825–850.
- Molteni, F., and T. N. Palmer, 1993: Predictability and finite-time instability of the northern winter circulation. *Quart. J. Roy. Meteor. Soc.*, **119**, 269–298.
- Noble, B., and J. W. Daniel, 1988: *Applied Linear Algebra*. 3d ed. Prentice-Hall, 521 pp.
- Palmer, T. N., R. Buizza, F. Molteni, Y.-Q. Chen, and S. Corti, 1994: Singular vectors and the predictability of weather and climate. *Philos. Trans. Roy. Soc. London*, **348A**, 459–475.
- Schoeberl, M. R., 1978: Stratospheric warmings: Observation and theory. *Rev. Geophys. Space Phys.*, **16**, 521–538.
- Simmons, A. J., and R. Strüfing, 1983: Numerical forecasts of stratospheric warming events using a model with a hybrid vertical coordinate. *Quart. J. Roy. Meteor. Soc.*, **109**, 81–111.
- Zeng, Q.-C., 1983: The evolution of a Rossby-wave packet in a three-dimensional baroclinic atmosphere. *J. Atmos. Sci.*, **40**, 73–84.